B 悪性神経膠腫の化学療法

神経膠腫は，浸潤性の発育をするため手術的に全摘することは不可能であり，術後の補助療法が不可欠である．しかしながら，膠芽腫（GBM）や退形成性星細胞腫（AA）などの悪性神経膠腫は，今なおきわめて予後不良な疾患であり，脳腫瘍全国統計による5年生存率は，それぞれ7％，23％にすぎない[1]．放射線治療の効果は認められるものの，それによる治癒は望めず，化学療法に至っては，nitrosourea以外に明らかな有効性を示すものがないといえ，その治療は困難をきわめている．新規経口アルキル化剤Temozolomide（TMZ）の出現は，悪性神経膠腫の治療においては画期的なことであり，膠芽腫に対し，単独薬剤として初めて統計的有意差をもって放射線単独治療の成績を上回り，当面，TMZを中心とした補助療法の開発が進むものと考えられる．

1 悪性神経膠腫に対する化学療法の歴史

悪性神経膠腫に対する大規模な化学療法の臨床試験が始められたのは1970年代でありWalkerらのBrain Tumor Study Groupがその先駆けとなっている[2]．血液脳関門の存在により，分子量が小さく，脂溶性薬剤を中心に臨床試験が行われ，静注用のBCNU（Carmustine，分子量214），経口投与のCCNU（Lomustine，分子量234），methyl CCNU（Semustine，分子量248）などが用いられた．いずれも単剤の効果が低いことから，放射線治療と併用した化学放射線治療としての効果が調べられた．放射線単独での治療効果については，Walkerらの報告があり，45 Gyから50，55，60 Gyと照射量をあげるに従って，生存期間中央値も13.5週，28.0週，36週，42週と延長するため，当時は全脳照射60 Gyが標準治療とされており，それにBCNU，methyl CCNUを加える形での治療が行われた．その結果，放射線単独治療，methyl CCNU併用放射線治療に比べ，有意差はないもののBCNU併用放射線治療の悪性神経膠腫の1年生存率は50.0％，2年生存が15.2％と最も良好であり，さらにChangらは，70 Gyの放射線単独での生存期間の延長はなく，BCNU併用放射線60 Gy照射において，40歳から60歳に限っていえば，有意に生存期間の延長があったことを報告し，欧米での標準治療はBCNU＋60 Gy全脳照射となった（表6-1）[3,4]．その後，放射線治療については，90％の膠芽腫症例において，原発病巣の周辺2 cm以内から再発がみられたというHochbergらの報告に基づき，放射線による高次脳機能障害の強い全脳照射から局所照射に変更された[5]．

一方，国内においては臨床試験の行える基盤が不十分で，大規模な臨床試験が行えない状況が続いた．唯一ともいえるのが，Takakuraらの報告である[6]．これは，GBMおよびAAを対象とした術後放射線単独治療とACNU（nimustine hydrochloride）を併用した放射線治療との第III相ランダム化比較試験である．放射線照射は局所に50 Gyないし60 Gy行われ，併用群については，照射期間中にACNU 100 mg/m^{2}が1～2回静脈内投与された．その結果，奏効率については併用群が47.5％で，放射線単独群の13.5％に比べ有意に優っていたが，生存率については，併用群が優っていたものの有意差を得るに至らなかった（表6-2）．

表 6-1 悪性神経膠腫 626 例の生存期間中央値 (Chang 1983)[4]

	age (years)			
	all	< 40	40 ~ 60	> 60
RT 60Gy	9.9 mo	30.4	9.3	5.4
RT 70Gy	8.4	23.7	8.7	6.2
RT 60Gy + BCNU	10.0	25.4	11.3	6.3
RT 60Gy + MeCCNU + DTIC	9.8	26.2	9.9	4.8

RT : radiotherapy, BCNU : carmustine, MeCCNU : semustine
DTIC : dacarbazine

表 6-2 悪性神経膠腫に対する ACNU および放射線治療の効果 (Takakura 1986)[6]

	Response rate	3-yr survival	
		AA	GBM
RT (n = 37)	13.5 %	48.9 %	0 %
RT + ACNU (n = 40)	47.5 %	59.0 %	16.3 %

AA : anaplastic astrocytoma, GBM : glioblastoma

2 悪性神経膠腫治療のスタンダード

2005 年 European Organisation for Research and Treatment of Cancer (EORTC) および National Cancer Institute of Canada (NCIC) から画期的な論文が発表された[7]. これは, GBM を対象とした第 III 相試験であり, 組織診断確定後 6 週間以内に, 無作為に放射線単独治療 (1 回 2 Gy で週 5 日, 総線量 60 Gy の分割照射) または放射線および TMZ 併用療法 (1 日 75 mg / m^2 を放射線治療期間中最長 49 日服用) さらに 6 コースの化学療法 (28 日ごとに 150 ~ 200 mg / m^2 を 5 日間) に割り付け, 1 週以内に治療を開始するというものである (図 6-8)[7]. 照射は肉眼的腫瘍体積に 2 ~ 3 cm のマージンを加えた部分を臨床標的体積とし, 治療計画は CT を用い, 3 次元計画システムを用いた. Primary endpoint は全生存期間, secondary endpoint は無増悪生存期間, 安全性, QOL とした. 15 カ国 85 施設から 573 例 (放射線単独群 286 例, 放射線 + TMZ 併用群 287 例) が登録され, その結果, 28 カ月の平均観察期間で, 生存期間中央値は併用群 14.6 カ月 (95 % 信頼区間 13.2 ~ 16.8), 放射線単独群 12.1 カ月 (95 % 信頼区間 11.2 ~ 13.0) であり, 2 年生存率は併用群 26.5 % (95 % 信頼区間 21.2 ~ 31.7 %), 単独群 10.4 % (95 % 信頼区間 6.8 ~ 14.1 %) であった. 併用群において死亡についてのハザード比 0.63 (95 % 信頼区間 0.52 ~ 0.75, log-rank test $p < 0.001$) であり, これは, 併用群が放射線単独群に比べ, 37 % 死亡の危険性が減少したことを示している. また, 無増悪生存期間は併用群 6.9 カ月 (95 % 信頼区間 5.8 ~ 8.2), 放射線単独群

JCLS 408-12844

図 6-B EORTC / NCIC による TMZ 併用放射線治療のプロトコール

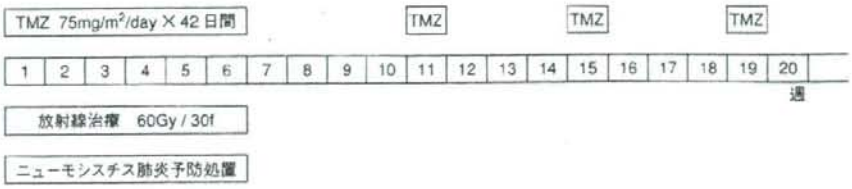

TMZ：放射線治療中　75mg/m²/day × 42 日間
維持化学療法　150 ～ 200mg/m²/day × 5 日間

5.0 カ月（95 %信頼区間 4.2 ～ 5.5）であり，ハザード比 0.54（95 %信頼区間 0.45 ～ 0.64）log-rank test $p < 0.001$ であった．放射線単独群では，grade 3 または 4 の血液毒性は認められなかったが，併用群では 12 例（4 %）に grade 3 または 4 の好中球減少，9 例（3 %）に血小板減少が観察された．最も高頻度にみられた非血液毒性は易疲労性であり，単独群で 26 %，併用群で 33 %に出現した．さらにその後の経過観察が報告され，単独放射線治療群の 2 年，3 年，4 年生存率が 11.2，4.3，3.8 %であったのに対し，併用群では 27.3，16.7，12.9 %であり，有意に併用群の生存率が優っていた[8]．

一方，国内でも AA 再発例に対し第 II 相試験が行われた．これは，初回再発のテント上 AA に対し，28 日ごとに 5 日間，初回 150 mg / m² の TMZ を経口投与し，その後は増量，減量基準に従い，100 ～ 200 mg / m² の TMZ を 5 日間投与するもので，32 例の登録症例において画像上 complete response 9 %，partial response 25 %で，奏効割合 34 %を示した．また，ステロイド使用，神経症状などを考慮した総合的腫瘍縮小効果では CR 3 %，PR 28 %であった．有害事象も欧米の報告と同様であったという結果に基づき，2006 年 9 月に国内でも使用が可能となった[9]．

3 国内における多施設共同試験

国内における臨床試験の基盤を作るため，2002 年渋井らは日本臨床腫瘍研究グループ（Japan Clinical Oncology Group，JCOG）内に脳腫瘍グループを立ち上げ，多施設共同試験を開始した．「星細胞腫 Grade 3 ・ 4 に対する放射線化学療法としての ACNU 単独療法と Procarbazine ＋ ACNU 併用療法とのランダム化第 II / III 相試験（JCOG 0305）」というタイトルで登録が開始され，2006 年 8 月までに 111 例（ACNU 群 55 例，Procarbazine ＋ ACNU 群 55 例）を集積した（図 6-9）[10]．この間，EORTC / NCIC の TMZ に関する前述のデータが発表され，世界的に標準治療が TMZ を併用した放射線治療に推移したことから，本試験を中止し，データ解析を進めている．この解析結果を待って，次の臨床試験としては TMZ を中心とした併用療法を計画している．

4 分子生物学的知見による化学療法

a) 1p，19q 欠失と退形成性乏突起膠腫の PCV 療法感受性

近年の分子生物学的手法の発達に伴い，治療法の選択にもその知見が応用されるようになった．

図 6-9 JCOG 0305 の study design（ランダム化第 II / III 相試験）

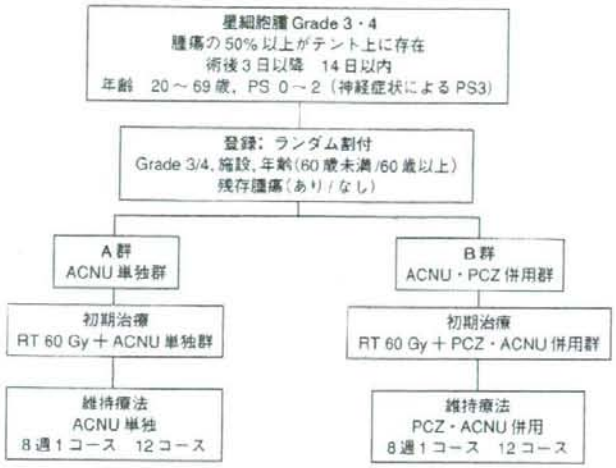

脳腫瘍領域では染色体 1 番短腕（1p）および 19 番長腕（19q）の欠失と退形成性乏突起膠腫に対する procarbazine＋CCNU＋vincristine（PCV 療法）の効果との関連性が指摘され，国内では CCNU の代わりに ACNU を用いた PAV 療法が多用されている[11]．しかしながら，CCNU と ACNU は同じ nitrosourea 系抗がん剤とはいっても別の薬剤であり，CCNU の効果をそのまま ACNU に当てはめることはできず，本来であれば PAV 療法について国内での臨床試験により，その効果を実証する必要がある．一方，2006 年に EORTC および RTOG から同時に PCV 療法の効果を疑問視する論文が発表された．これは退形成性乏突起膠腫に対する術後治療として，放射線治療単独群と PCV 併用放射線治療群との効果を 1p，19q 欠失の有無により比較したもので，いずれの発表でも無増悪生存率に差を認めたものの全生存期間で差がなかったというものである（**図 6-10**）．すなわち，1p，19q 欠失は PCV 療法に対する感受性を示すものではなく，放射線治療にも同様に反応するという治療感受性を示す因子であることが証明されたことになる[12,13]．

b) MGMT と TMZ の治療効果

Nitrosourea 系抗がん剤の耐性機構の一つである O6-methylguanine-DNA methyltransferase（MGMT）遺伝子の存在と抗腫瘍効果は，以前より注目されており，前述の JCOG 0305 の臨床試験もこの理論に基づいたもので，procarbazine 投与により MGMT が低下し ACNU の治療効果が高まることを期待した治療法である[11]．EORTC の臨床試験での TMZ による治療においても同様な治療効果の差が報告されている．MGMT promoter がメチル化されている（MGMT が発現していない）GBM 症例に対し TMZ 併用放射線治療を行った場合の生存期間中央値は 21.7 カ月であり，メチル化されていない（MGMT が発現している）GBM 症例に対し同じ治療を場合の 12.7 カ月に比べ有意に延長している[15]．すなわち，腫瘍を摘出した段階で，この治療による効果を予測でき

図 6-10 EORTC による 1p，19q 欠失と PCV 療法の効果との関連性

左：無増悪生存期間，右：全生存期間（Van den Bent, 2006）[12]

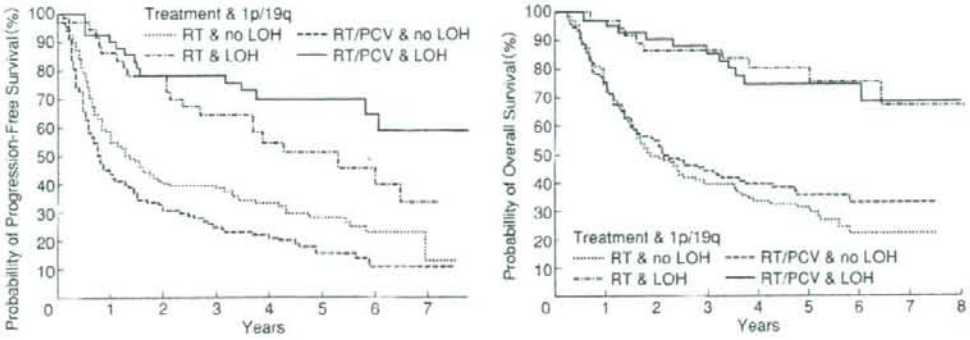

図 6-11 MGMT メチル化の有無による GBM 生存率

(Hegi, 2005)[5]

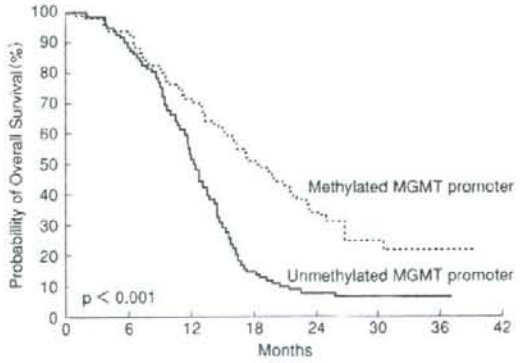

ることになる．GBM に対する標準治療が TMZ 併用放射線治療となっている現時点で，MGMT のメチル化が認められないからといって，他の治療法を第 1 選択とすることはできないが，初期治療および維持療法初期の反応性をみて，十分な治療効果が認められない場合には，早期に他の治療法への移行を考える材料となり得る．

おわりに

ここ数十年，全くといっていいほど進歩のみられなかった悪性神経膠腫の治療成績も TMZ の出現により，新しいエビデンスが生まれ，確実に一歩前進したといえる．しかしながら，TMZ を用いても GBM の生存期間中央値は 14.6 カ月にすぎず，他臓器の悪性腫瘍と比べ遙かに短いといえ

る．当面，TMZを中心した治療法の開発が進められると考えられるが，その際も分子生物学的知見を十分に取り入れ，より有効な症例の選択をするとともに，TMZ抵抗性の腫瘍に対する治療法の開発も同時に進めていかなければならない．そのためにも国内にも世界に発信できるエビデンスを構築するに足る臨床試験の体制を整備していくことが重要である．

■文献

1) Committee of Brain Tumor Registry of Japan. Report of Brain Tumor Registry of Japan (1969-1996). 11th ed. Neurol Med-Chir. 40suppl, 2003.
2) Walker MD, Strike TA, Sheline GE. An analysis of dose-effect relationship in the radiotherapy of malignant gliomas. Int J Radiation Oncology Biol Phys. 1979; 5: 1725-31.
3) Walker MD, Green SB, Byar DP, et al. Randomized comparisons of radiotherapy and nitrosoureas for the treatment of malignant glioma after surgery. N Engl J Med. 1980; 303: 1323-29.
4) Chang CH, Harton J, Schoenfeld D, et al. Comparison of postoperative radiotherapy and combined postoperative radiotherapy and chemotherapy in the multidisciplinary management of malignant gliomas. Cancer. 1983; 52: 997-1007.
5) Hochberg FH, Pruitt A. Assumptions in the radiotherapy of glioblastoma. Neurology. 1980; 30: 907-11.
6) Takakura K, Abe H, Tanaka R, et al. Effect of ACNU and radiotherapy on malignant gliomas. J Neurosurg. 1986; 64: 53-7.
7) Stupp R, Mason WP, van den Bent MJ, et al. Radiotherapy plus concomitant and adjuvant temozolomide for glioblastoma. N Engl J Med. 2005; 352: 987-96.
8) Mirimanoff R, Mason W, Van den Bent M, et al. Is long-term survival in glioblastoma possible ? Updated results of the EORTC/NCIC phase III randomized trial on radiotherapy (RT) and concomitant and adjuvant temozolomide (TMZ) versus RT alone. Int J Radiat Oncol Biol Physics. 2007; 69: Plenary-3, S2.
9) 西川 亮，渋井壮一郎，丸野元彦，他．初回再発の退形成性星細胞腫患者に対するTemozolomide単剤投与の有効性および安全性の検討―多施設共同第Ⅱ相試験―．癌と化学療法．2006; 33: 1279-85.
10) Shibui S. A randomized controlled trial on malignant brain tumors. The activities of Japan Clinical Oncology Group (JCOG)-Brain Tumor Study Group (BTSG). Neurol Med Chir. 2004; 44: 220-1.
11) Cairncross JG, Ueki K, Zlatescu MC, et al. Specific genetic predictors of chemotherapeutic response and survival in patients with anaplastic oligodendrogliomas. J Natl Cancer Inst. 1988; 90: 1473-9.
12) Van den Bent ML, Carpentier AF, Brandes AA, et al. Adjuvant procarbazine, lomustine, and vincristine improves progression-free survival but not overall survival in newly diagnosed anaplastic oligodendrogliomas and oligoastrocytomas: a randomized European Organisation for Research and Treatment of Cancer Phase III trial. J Clin Oncol. 2006; 24: 2715-22.
13) Cairncross G, Berkey B, Shaw E, et al. Phase III trial of chemotherapy plus radiation compared with radiotherapy alone for pure and mixed anaplastic oligodendroglioma: Intergroup Radiation Therapy Oncology Group Trial 9402. J Clin Oncol. 2006; 24: 2707-14.
14) Brandes AA, Turazzi S, Basso U, et al. A multidrug combination designed for reversing resistance to BCNU in glioblastoma multiforme. Neurology. 2002; 58: 1759-64.
15) Hegi ME, Diserens AC, Gorlia T, et al. MGMT gene silencing and benefit from temozolomide in glioblastoma. N Engl J Med. 2005; 352: 997-1003.

<渋井壮一郎>

JCLS 498-12844

J Neurosurg Pediatrics 1:148–151, 2008

Desmoplastic infantile astrocytoma and characteristics of the accompanying cyst

Case report

TAKAAKI BEPPU, M.D.,[1] YUICHI SATO, M.D.,[1] NORIYUKI UESUGI, M.D.,[2] YASUTAKA KUZU, M.D.,[1] KUNIAKI OGASAWARA, M.D.,[1] AND AKIRA OGAWA, M.D., PH.D.[1]

Departments of [1]Neurosurgery and [2]Pathology, Iwate Medical University, Morioka, Japan

✓A desmoplastic infantile astrocytoma (DIA) is an extremely rare tumor that comprises a solid astrocytic tumor accompanied by a large cyst and involves the superficial cerebral cortex and leptomeninges in infants. The solid part of this type of tumor has been well described in various reports and books, but characteristics of the cystic portion have remained unclear. Because adequate resection is required to ensure a favorable prognosis, information about the cyst is very important for diagnostic purposes and surgical planning. The authors report on the clinical and histological features of the cyst in a case of a DIA. A 12-month-old boy presented with vomiting. Contrast-enhanced magnetic resonance imaging revealed a strongly enhancing single-lobed large cyst located in the deep white matter, under the solid part of the tumor attached to the dura mater of the left frontal lobe. Both the solid and cystic portions of the tumor were surgically removed. The border between the cyst wall and surrounding white matter was unclear. Histologically, the cyst wall was composed of gliosis representing a rough accumulation of reactive astrocytes, lymphocytes, and small capillary vessels in edematous parenchyma, but no tumor cells. The present case and previous reports suggest that the cyst does not contain tumor cells, even if strongly depicted on contrast-enhanced neuroimaging, and that a thickly enhancing cyst wall indicates gliosis with accumulation of numerous small vessels. *(DOI: 10.3171/PED/2008/1/2/148)*

KEY WORDS • **cyst** • **desmoplastic infantile astrocytoma** • **desmoplastic infantile ganglioglioma** • **histology** • **magnetic resonance imaging** • **pediatric neurosurgery**

A DIA, originally referred to as a "superficial cerebral astrocytoma attached to dura with desmoplastic reaction" or "desmoplastic cerebral astrocytoma of infancy," has been defined as a large cystic astrocytic tumor in infants that involves the superficial cerebral cortex and leptomeninges, often attaching to the dura mater, with a generally good prognosis following adequate resection.[21,22] Both a DIA and a DIG have been integrated into the same tumor type class in the World Health Organization classification system, as both tumors display similar clinical and pathological features, excluding involvement of a variable neuronal component together with astrocytes in a DIG.[21] The solid part of the tumor is easily removed due to the location and clear demarcation from surrounding brain tissue.[20] Because surgical removal of the tumor leads to favorable prognosis, neurosurgeons play a large role in the treatment of a DIA and DIG. Although both a DIA and DIG are very rare, characteristics of the solid part of the tumor have been well described.[4,17,22] In contrast, characteristics of the cyst have remained unclear. For neurosurgeons, general information on clinical and histopathological features of the cyst is important for diagnosis and treatment. The current report describes a case of a DIA with a large cyst, and reviews clinical and histological findings of DIA cysts in the literature.

Abbreviations used in this paper: DIA = desmoplastic infantile astrocytoma; DIG = desmoplastic infantile ganglioglioma; MR = magnetic resonance.

Case Report

History and Examination. This 12-month-old boy was born at term after an uncomplicated pregnancy and delivery. His perinatal course was normal. One month before admission, he presented with vomiting. On admission, an examination revealed a head circumference of 50.3 cm (greater than the mean plus 2 standard deviations) but no neurological deficits. His medical history included no episodes suggestive of

systemic autoimmune disease, intracranial infection, or head injury, and revealed no previous surgery or radiation treatment. Physical and blood serum examinations revealed no abnormalities.

Magnetic resonance was performed, and T1- and T2-weighted imaging revealed a circumscribed solid lesion located superficially in the cortex of the left frontal lobe, and a large cyst in the deep white matter medial to the solid tumor. The T1- and T2-weighted imaging also showed isointense and very low signals, respectively. Gadolinium-enhanced T1-weighted imaging revealed homogeneous enhancement in the solid part of the tumor with the exception of the central region (Fig. 1). A large single-lobed cyst (maximum diameter 5.5 cm) accompanied the solid part of the tumor. Fluid in the cyst displayed greater signal intensity than cerebrospinal fluid. The thick cyst wall also displayed strong enhancement on gadolinium-enhanced T1-weighted imaging (Fig. 1). Computed tomography depicted no calcified foci in the solid part of the tumor or in the cyst wall. Left internal carotid angiography revealed slight intratumoral neovascularity fed from the operculum artery, whereas no intratumoral neovascularity was found on external carotid angiography.

Operation and Postoperative Course. A skin incision and craniotomy were performed at the region of presumed exposure of the tumor. Before opening the dura, xanthochromic fluid in the cyst was aspirated using ultrasonographic guidance until sufficient relaxation of the frontal lobe was achieved. Upon opening, the dura did not firmly adhere to the solid part of the tumor. The meningioma-like hard and reddish-gray solid portion was well demarcated due to preservation of arachnoid matter adjacent to the tumor, and was easily separated from surrounding cortex and edematous white matter. After removal of the solid portion, the cyst wall was noted to consist of a soft and gliotic membrane with a reddish-gray color. Although the cyst could be removed completely, separation of the cyst wall from surrounding white matter was more difficult than removal of the solid portion, because the border between the cyst wall and surrounding white matter was unclear. We dissected between the cyst and surrounding white matter using an ultrasonic surgical aspirator. Postoperative MR imaging demonstrated that both the solid and cystic portions of the tumor had been completely removed.

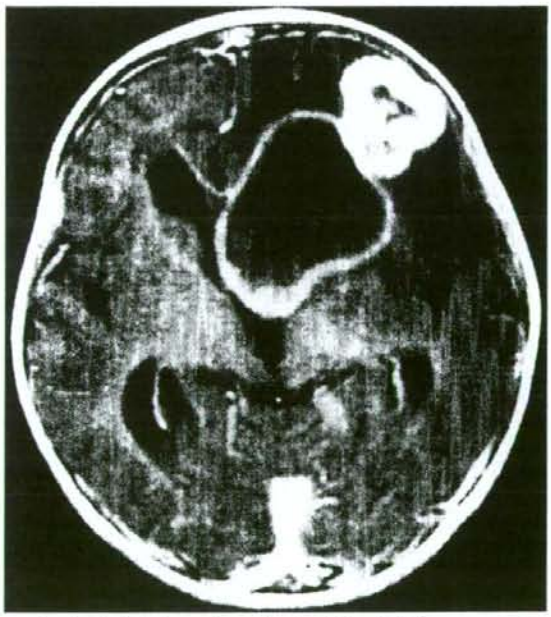

FIG. 1. Gadolinium-enhanced T1-weighted MR image reveals a heterogeneous enhancing mass attached to the dura in the left frontal convex. The mass accompanies a large and thickly enhancing cyst in the deep white matter.

Histology. The removed solid part of the tumor revealed typical histological features of proliferating spindle-shaped cells intermingling with large amounts of collagenous stroma showing storiform or whorled patterns (Fig. 2 *upper*). The collagenous stroma displayed positive results for silver staining. Spindle-shaped cells were immunohistochemically positive for glial fibrillary acidic protein. No necrosis, mitosis, calcified focus, or synaptophysin-positive ganglion cells were seen anywhere in the tumor. The histological diagnosis of the tumor was a DIA.

The cyst wall demonstrated histological features of gliosis, with numerous small round cells such as astrocytes and lymphocytes, and numerous small vessels scattered in edematous parenchyma. Reactive gliosis was observed in the surrounding white matter (Fig. 2 *lower*). In particular, small vessels had accumulated close to the outside of the cyst wall. The cyst wall and brain tissue adjacent to the tumor were thoroughly positive for glial fibrillary acidic protein. Examination of the entire cyst wall, however, revealed no tumor cells.

Discussion

The DIA and DIG tumor types are extremely rare. Only 31 cases of a DIA have been reported in the literature.[1,3,5–19,21,22,24] The tumor was accompanied by a cyst in 30 of 32 cases (93.8%), including the present case. The DIA comprised a solid tumor without a cyst in only 2 cases.[8,18] Cyst size was defined in 15 cases from 9 reports (including the present study) and varied widely between 1.5 and 12 cm (mean 9.3 cm). The cyst in a DIA is most frequently composed of a single lobule on preoperative neuroimaging as in the present case, rather than multiple lobules separated by septa. Reports have described cysts with 1, 2, and 3 lobules in 10, 3,[7,16,17] and 2 cases,[14,19] respectively. The solid part of a DIA is frequently located at the superficial cerebrum, and the cyst has been located in the deep cerebrum under the solid portion in almost all previous cases. In 19 cases for which cyst location was defined,[1,3,6,7,9,10,13–17,19,21,22,24] only 3 cases revealed the cyst to be in a location other than deep white matter medial to the solid part of the tumor.[10,19,24]

The cyst in the present case possessed a thick wall in addition to strong enhancement on gadolinium-enhanced T1-weighted imaging. Results from previous studies, however, have suggested that the cyst wall was obscure and lacked enhancement on contrast-enhanced computed tomography scans or MR images.[19,23] In the literature, 15 reports have described findings on contrast-enhanced computed tomography scans or MR images, with 11 cases demonstrating

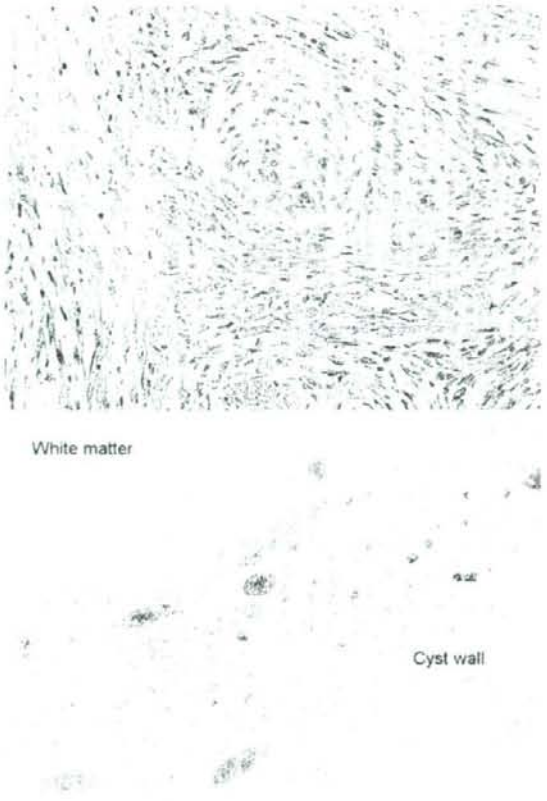

FIG. 2. Photomicrographs of the histological features of the solid *(upper)* and cystic *(lower)* portions of the tumor. *Upper:* The solid part of the tumor displays typical histological features with proliferation of spindle-shaped cells intermingling with a large amount of collagenous stroma showing storiform or whorled patterns. *Lower:* The cyst wall displays scattered small round cells such as astrocytes and lymphocytes, and small capillary vessels in edematous parenchyma. White matter adjacent to the cyst also demonstrates the same round cells. Capillary vessels are accumulated more in the outer cyst wall. H & E, original magnification × 100 *(upper)* and × 40 *(lower)*.

obscure or unenhanced cyst walls and 4 cases showing thickly enhancing cyst walls.[6,11,14,17] The cyst wall in the present case did not contain tumor cells in sections stained using H & E. Some reports have described histological features of the cyst wall. Kurose and coauthors[10] reported that a thickly enhancing cyst wall in a case of DIA did not contain tumor cells but showed scattered xanthoma cells with normal morphological features. Sugiyama and associates[20] reported 4 cases in a mixed series of DIA and DIG cases, and also noted that cyst walls were free of invading tumor cells. Kim et al.[7] observed no tumor cells within the septum of a multilobular cyst in a case involving a DIA. No reports have found tumor cells in the cyst wall of a DIA. An obscure and nonenhancing cyst wall in a DIA case showed macroscopically gliotic characteristics during surgery according to de Chadarévian and coworkers.[3] In the present case, macroscopic observation of the cyst wall revealed gliotic characteristics during surgery, and the cyst wall histologically demonstrated the features of gliosis, with numerous scattered round cells such as astrocytes and lymphocytes, and small vessels in edematous parenchyma. We speculate that enhancement of the cyst wall on neuroimaging is induced by accumulation of the small vessels within the area of gliosis, or increasing permeability of the blood–brain barrier in vessels due to gliosis. Kandalkar and colleagues[5] reported that the histology of the cyst wall in a case of a DIA showed normal but atrophic brain tissues in which the outer layer was increased due to gliosis, although results of neuroimaging were not demonstrated. They speculated that these histological changes in the cyst resulted from pressure of cyst fluid on the adjacent brain, and recommended excision of the cyst portion for seizure control after surgery. In the present case, gliosis was increased within the outer cyst wall, and was observed in adjacent white matter tissue. The border between the cyst wall and surrounding white matter was unclear. This adhesion between the cyst wall and surrounding white matter might be induced by aggressive gliosis within the outer side of the wall. The deep location, large size, and unclear border of the cyst may complicate removal of the cystic portion compared with the solid portion. Gross-total removal of a DIA or DIG leads to a favorable prognosis, but long-term survival is anticipated even with residual disease.[21,22] It needs to be emphasized that surgery for DIA only requires removal of the solid portion of the tumor when the cyst wall is nonenhanced on neuroimaging. This approach is similar to the surgical plan for a pilocytic astrocytoma, in which neurosurgeons generally assume that the cyst wall is not neoplastic or does not require resection.[2] Based on findings from the present case and the literature, we also believe that surgery for a DIA with a thickly enhancing cyst wall only requires removal of the solid portion of the tumor and that removal of the cyst wall is not necessary. If the residual cyst wall causes uncontrollable seizures after surgery, a second operation to remove the cyst wall should be considered.

Conclusions

Cyst characteristics of a DIA or DIG do not appear to have been fully explored in previous studies. Because surgery plays a large role in treatment for a DIA and DIG, characteristics of the cyst commonly located in the deep white matter under the solid part of the tumor represent important information for neurosurgeons. Clinical and histological findings in the present case and previous reports suggest that the cyst does not contain tumor cells, even if strong enhancement is seen on contrast-enhanced neuroimaging, and that a thickly enhancing cyst wall indicates gliosis with accumulation of numerous small vessels. The border between the cyst wall and surrounding white matter is unclear compared with the border between the solid portion and surrounding cortex. We therefore believe that the cyst wall does not require removal during surgery for a DIA, even when the cyst wall is thickly enhanced on neuroimaging. Further study of the cyst wall in a limited group of patients with a DIA or DIG is required to confirm our distinct impressions.

Acknowledgment

We thank Prof. Shinichi Nakamura of the Department of Pathology, Iwate Medical University, for performing the histological examination in the present case.

References

1. Aydin F, Ghatak NR, Salvant J, Muizelaar P: Desmoplastic cerebral astrocytoma of infancy. A case report with immunohistochemical, ultrastructural and proliferation studies. **Acta Neuropathol (Berl) 8:**666–670, 1993
2. Burger PC, Scheithauer BW, Paulus W, Szymas J, Giannini C, Kleihues P: Pilocytic astrocytoma, in Kleihues P, Cavenee WK (eds): **World Health Organization of Tumours. Pathology and Genetics: Tumours of the Nervous System.** Lyon: IARC Press, 2000, pp 45–51
3. de Chandarévian JP, Pattisapu JV, Faerber EN: Desmoplastic cerebral astrocytoma of infancy. Light microscopy, immunocytochemistry, and ultrastructure. **Cancer 66:**173–179, 1990
4. Grundy R, Mallucci C: Rare tumors, in Walker DA, Perilongo G, Punt JAG, et al (eds): **Brain and Spinal Tumors of Childhood.** London: Arnold, 2004, pp 397–416
5. Kandalkar B, Shah V, Shet T: Desmoplastic astrocytoma of infancy—a case report. **Indian J Pathol Microbiol 44:**329–332, 2001
6. Kato M, Yano H, Okumura A, Shinoda J, Sakai N, Shimokawa K: A non-infantile case of desmoplastic infantile astrocytoma. **Childs Nerv Syst 20:**499–501, 2004
7. Kim JH, Kim IO, Kim WS, Kim KH, Park CM, Yeon KM: MR findings of desmoplastic cerebral astrocytoma of infancy. **Acta Radiol 44:**688–690, 2003
8. Kopniczky Z, Kóbor J, Maráz A, Vajtai I: Desmoplastic neuroepithelial tumor of infancy in the nevus sebaceus syndrome: report of a unique constellation and review of the literature. **Pathol Res Pract 197:**279–284, 2001
9. Kros JM, Delwel EJ, de Jong TH, Tanghe HL, van Run PR, Vissers K, et al: Desmoplastic infantile astrocytoma and ganglioglioma: a search for genomic characteristics. **Acta Neuropathol (Berl) 104:**144–148, 2002
10. Kurose A, Beppu T, Miura Y, Suzuki M, Ogawa A, Arai H, et al: Desmoplastic cerebral astrocytoma of infancy intermingling with atypical glial cells. **Pathol Int 50:**744–749, 2000
11. Louis DN, von Deimling A, Dickersin GR, Dooling EC, Seizinger BR: Desmoplastic cerebral astrocytomas of infancy: a histopathologic, immunohistochemical, ultrastructural, and molecular genetic study. **Hum Pathol 23:**1402–1409, 1992
12. Mallucci C, Lellouch-Tubiana A, Salazar C, Cinalli G, Renier D, Sainte-Rose C, et al: The management of desmoplastic neuroepithelial tumors in childhood. **Childs Nerv Syst 16:**8–14, 2000
13. Olas E, Kordek R, Biernat W, Liberski PP, Zakrzewski K, Alwasiak J, et al: Desmoplastic cerebral astrocytoma of infancy: a case report. **Folia Neuropathol 36:**45–51, 1998
14. Park K, Yoo J, Cho H, Cho W, Park S: Desmoplastic cerebral astrocytoma of infancy: a case report. **J Korean Med Sci 13:** 440–444, 1998
15. Paulus W, Schlote W, Perentes E, Jacobi G, Warmuth-Metz M, Roggendorf W: Desmoplastic supratentorial neuroepithelial tumors of infancy. **Histopathology 21:**43–49, 1992
16. Rodriguez-Morales EL, Correa Rivas MS, Colon CE: Desmoplastic astrocytoma of infancy: a case report with histopathologic and immunohistochemistry profile. **P R Health Sci J 21:** 129–132, 2002
17. Rosenblum MK: Desmoplastic infantile astrocytoma/desmoplastic infantile ganglioglioma, in McLendon RE, Rosenblum MK, Bigner DD (eds): **Russell and Rubinstein's Pathology of Tumors of the Nervous System, ed 7.** London: Hodder Arnold, 2006, pp 321–332
18. Rushing EJ, Rorke LB, Sutton L: Problems in the nosology of desmoplastic tumors of childhood. **Pediatr Neurosurg 19:**57–62, 1993
19. Serra A, Strain J, Ruyle S: Desmoplastic cerebral astrocytoma of infancy: report and review of the imaging characteristics. **AJR Am J Roentgenol 166:**1459–1461, 1996
20. Sugiyama K, Arita K, Shima T, Nakaoka M, Matsuoka T, Taniguchi E, et al: Good clinical course in infants with desmoplastic cerebral neuroepithelial tumor treated by surgery alone. **J Neurooncol 59:**63–69, 2002
21. Taratuto AL, Monges J, Lylyk P, Leiguarda R: Superficial cerebral astrocytoma attached to dura. Report of six cases in infants. **Cancer 54:**2505–2512, 1984
22. Taratuto AL, VandenBerg SR, Rorke LB: Desmoplastic infantile astrocytoma and ganglioglioma, in Kleihues P, Cavenee WK (eds): **World Health Organization of Tumours. Pathology and Genetics: Tumours of the Nervous System.** Lyon: IARC Press, 2000, pp 99–102
23. Trehan G, Bruge H, Vinchon M, Khalil C, Ruchoux MM, Dhellemmes P, et al: MR imaging in the diagnosis of desmoplastic infantile tumor: retrospective study of six cases. **AJNR Am J Neuroradiol 25:**1028–1033, 2004
24. Vajtai I: Desmoplastic cerebral astrocytoma in intraventricular location: simplifying histogenesis by broadening the spectrum of desmoplastic neuroepithelial tumors of infancy? **AJR Am J Roentgenol 168:**1385, 1997

Manuscript submitted July 29, 2007.
Accepted September 26, 2007.
This work was supported by the Advanced Medical Science Center, Iwate Medical University, Morioka, Japan.

Address correspondence to: Takaaki Beppu, M.D., Department of Neurosurgery, Iwate Medical University, 19-1 Uchimaru, Morioka 020-8505, Japan. email: tbeppu@iwate-med.ac.jp.

Neurol Med Chir (Tokyo) 48, 418 – 422, 2008

Fusion of Magnetic Resonance Angiography and Magnetic Resonance Imaging for Surgical Planning for Meningioma

—Technical Note—

Hiroshi KASHIMURA, Kuniaki OGASAWARA, Hiroshi ARAI, Takaaki BEPPU, Takashi INOUE*, Tsutomu TAKAHASHI**, Koichi MATSUDA**, Yujiro TAKAHASHI**, Shunrou FUJIWARA***, and Akira OGAWA

*Department of Neurosurgery, Iwate Medical University School of Medicine, Morioka, Iwate; *Department of Neurosurgery, Kohnan Hospital, Sendai, Miyagi; **Software and Information Science, Iwate Prefectural University, Iwate; ***Advanced Medical Research Center, Takizawa, Iwate*

Abstract

A fusion technique for magnetic resonance (MR) angiography and MR imaging was developed to help assess the peritumoral angioarchitecture during surgical planning for meningioma. Three-dimensional time-of-flight (3D-TOF) and 3D-spoiled gradient recalled (SPGR) datasets were obtained from 10 patients with intracranial meningioma, and fused using newly developed volume registration and visualization software. Maximum intensity projection (MIP) images from 3D-TOF MR angiography and axial SPGR MR imaging were displayed at the same time on the monitor. Selecting a vessel on the real-time MIP image indicated the corresponding points on the axial image automatically. Fusion images showed displacement of the anterior cerebral or middle cerebral artery in 7 patients and encasement of the anterior cerebral arteries in 1 patient, with no relationship between the main arterial trunk and tumor in 2 patients. Fusion of MR angiography and MR imaging can clarify relationships between the intracranial vasculature and meningioma, and may be helpful for surgical planning for meningioma.

Key words: three-dimensional time-of-flight magnetic resonance angiography, magnetic resonance imaging, meningioma, fusion imaging

Introduction

Surgical planning for meningioma requires information about the peritumoral angioarchitecture, in addition to the tumor consistency, location, and size,[5,12] because the involvement or course of any adjacent arteries affects the surgical outcome in tumors located at the skull base or eloquent areas.[6] Magnetic resonance (MR) imaging provides good spatial resolution and excellent contrast with soft tissues, but does not allow detailed analysis of the cerebral vasculature. MR angiography provides just such information on cerebral vasculature.[2] Therefore, fusing of the MR angiograms and MR images may enable simultaneous visualization of the intracranial vasculature and brain tissues.

The present study developed a fusion technique for MR angiography and MR imaging that could facilitate surgical planning for meningioma.

Received November 19, 2007; Accepted April 22, 2008

Technical Description

MR imaging was performed with a Signa VH/i 3.0 T scanner (General Electric Systems, Milwaukee, Wis., U.S.A.) and a parallel imaging head coil. Three-dimensional time-of-flight (3D-TOF) MR angiography was performed using conventional single-slab acquisition in all patients. The pulse sequence was as follows: repetition time (TR), 30 msec; echo time (TE), 3.9 msec; flip angle, 60°; matrix size, 512 × 256; field of view (FOV), 22 × 17 cm; slice thickness, 1.2 mm; 1 averaged with an acquisition time of 11 minutes 12 seconds. Then, 3D-spoiled gradient recalled (SPGR) MR imaging was acquired using the following: TR, 11.3 msec; TE, 2.2 msec; flip angle, 15°; matrix size, 512 × 256; FOV, 22 × 22 cm; slice thickness, 1.2 mm; 1 averaged with an acquisition

time of 5 minutes 35 seconds.

The 3D-TOF and 3D-SPGR datasets were fused on a personal computer using volume registration and visualization software that we developed. This original software was implemented with C/C++ on Windows by one of the authors (T.T.). The software supports the following formats: DICOM and ANALYZE 7.5. Coordination between the two volume datasets was manually adjusted if required, although 3D-TOF and 3D-SPGR were performed sequentially. The registration procedure started with manual designation of a predefined anatomic point in both modalities. This procedure requires rigid-motion transformation (rotation, translation, scaling) between 3D-MR imaging and 3D-MR angiography. Scaling can be derived from knowledge of the voxel sizes in both modalities, so only rotation and translation had to be estimated from the data. Therefore, new volume registration software was developed to rotate and translate one volume dataset through a graphical user interface to visualize two volume datasets in different colors within the same 3D space using real-time volume rendering. All volume registration was successfully performed within 15 minutes per patient.

Using this software, the maximum intensity projection (MIP) of 3D-TOF MR angiography and axial SPGR MR imaging were displayed simultaneously on the monitor. Selecting the vessel on the real-time MIP image with the mouse resulted in software indicating the corresponding points on the axial image automatically. Using this method, we could evaluate the accuracy of registration between vessels in 3D-MR angiography and hyperintense areas on axial MR imaging, which corresponded to the vessels on SPGR MR images.

The software was based on a new algorithm for visualizing vessel tracts. A green line was traced along the vessels on the MIP images in 3D space and the green line was shown simultaneously on the axial SPGR MR image as a red point. In addition, the positions of vessels could also be visualized on 3D-MR angiography by selecting the corresponding vessels on the two-dimensional (2D) image. Therefore, the correspondence between any artery on 3D-MR angiography and a hyperintense spot or string on axial MR imaging could easily be demonstrated in real time.

Results

MR fusion imaging was successfully performed within 15 minutes in a total of 10 patients, 7 women and 3 men aged 29–73 years (mean 54.9 years), with meningioma between December 2006 and April 2007 (Table 1). The tumor was located in the convex in 4 patients, the falx in 1, the cerebellar tentorium in 1, the petroclivus in 1, the temporal base in 1, the olfactory groove in 1, and the tuberculum sellae in 1. All tumors were surgically resected

Table 1 Summary of 10 patients

Case No.	Age (yrs)/ Sex	Tumor location	Tumor size (cm)	Peritumoral angioarchitecture			Postoperative new neurological deficits
				Arteries distant from the tumor	Arteries running along the tumor	Arteries perforating the tumor	
1	48/F	lt cerebellar tentorium	5.4×5	BA, lt SCA, lt PCA			no
2	73/F	rt parietal falx	4×3.5			rt ACA branches	no
3	29/F	rt convex	7×7		bil A_2-A_3		no
4	69/F	lt petroclivus	3×3	BA, lt SCA			lower CN palsy
5	38/M	lt parietal convex	8.8×6		lt ACA branch, lt MCA branch		no
6	71/M	rt frontal convex	8.8×6		rt A_2-A_3		no
7	68/M	lt parietal convex	4×3		lt MCA branches		no
8	59/F	lt temporal base	5.2×3.2		lt MCA branches		no
9	59/F	olfactory groove	5.5×5.5		bil A_2-A_3		no
10	35/F	tuberculum sellae	2.5×2.5		bil ICAs, rt M_1, bil ACAs		no

ACA: anterior cerebral artery, BA: basilar artery, CN: cranial nerve, ICA: internal carotid artery, MCA: middle cerebral artery, PCA: posterior cerebral artery, SCA: superior cerebellar artery.

and histological diagnoses were established. Appropriate informed consent was obtained from each patient or their relatives.

Fusion images showed displacement of the anterior cerebral artery (ACA) or middle cerebral artery in 7 patients and encasement of the ACA in 1 patient (Table 1). No relationship was seen between the main arterial trunk and the tumor in the remaining 2 patients. The relationship between tumor and arteries corresponded with intraoperative findings in all cases. Only 1 of the 10 patients experienced new neurological deficits, as Case 4 developed lower cranial nerve palsy. However, the symptoms gradually improved. Postoperative MR imaging showed no new ischemic lesions in any patient.

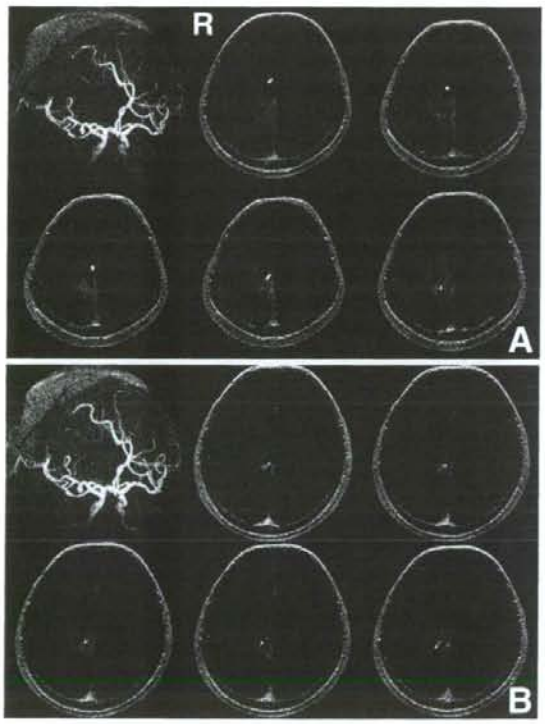

Fig. 1 Case 2, a 73-year-old woman with atypical meningioma. The *green line* was drawn on the anterior cerebral artery (ACA) on the maximum intensity projection image in three-dimensional space and the location of the *green line* was shown simultaneously on axial spoiled gradient recalled magnetic resonance images as a *red point*. The distal branches of the right ACA entered the tumor anteriorly (A) and inferiorly (B), but did not penetrate the tumor.

Illustrative Cases

Case 2: A 73-year-old woman presented with progressive left leg monoparesis over a period of 1 year. MR imaging revealed heterogeneous enhancement of the tumor attached to the falx in the right cerebral hemisphere. MR fusion imaging clearly showed that the distal branches of the right ACA entered the tumor anteriorly and inferiorly, but did not penetrate the tumor (Fig. 1). Intraoperatively, encased vessels were also confirmed and resected. The tumor was totally resected with the attached falx.

Case 3: A 29-year-old woman presented with a 10-year history of recurrent headache. MR imaging revealed heterogeneous enhancement of the tumor attached to the convex and falx in the right cerebral hemisphere. MR fusion imaging clearly showed that the A_2 and A_3 segments of the bilateral ACAs were displaced and ran along the posterior part of the tumor (Fig. 2). We confirmed and preserved the bilateral ACAs during surgery.

Discussion

This study showed that the new technique for fusing MR angiography and MR imaging allows clarification of the relationship between the intracranial vasculature and meningioma, which facilitates the sur-

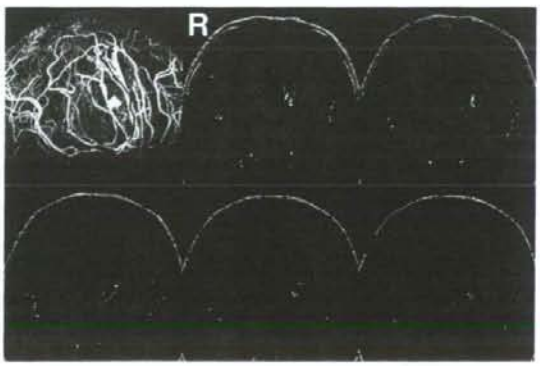

Fig. 2 Case 3, a 29-year-old woman with transitional meningioma. The *green line* was drawn on the anterior cerebral artery (ACA) on the maximum intensity projection image in three-dimensional space and the location of the *green line* was shown simultaneously on axial spoiled gradient recalled magnetic resonance images as a *red point*. The A_2 and A_3 segments of bilateral ACAs were displaced and ran along the posterior part of the tumor.

gical planning.

Recently, image fusion techniques for registering different kinds of images have been developed in neuroimaging.[4,8] The interest in image fusion is based on the idea that creating a fused image combining multiple modalities may provide more information than analysis of these modalities separately. Previous studies have reported the combination of MR imaging with computed tomography (CT), intracranial echography, single photon emission CT, and positron emission tomography.[4,8] Image fusion using 3D digital subtraction angiography (3D-DSA) and 3D-MR imaging provides information about both intracranial soft tissues and vasculature, and can visualize any perforating artery visible on 3D-DSA. Selecting any point on any of the 3D-DSA, and axial, coronal, and sagittal MR images can indicate the corresponding point on all the 3 other images.[7] 3D-DSA is the best technique to provide anatomical details of the vasculature,[3,9] but is invasive and involves a risk of neurological complications.[1,10]

The present software fuses 2D-MR imaging with MR angiography to trace the vessels in 3D space and indicate the location of the vessel on the axial image simultaneously. This technique can easily demonstrate in real time which arteries on 3D-MR angiography correspond to hyperintense spots or strings on axial MR imaging, and vice versa. This technique is very useful for clarifying spatial relationships between the adjacent vasculature and lesions on axial MR imaging.

Fusion imaging as described here offers the advantage that different kinds of images can be obtained from the same modality. Registration procedures are thus readily performed. In contrast, the present technique possesses some limitations. While MR angiography can demonstrate arterial main trunks, the visibility of important smaller vessels such as the lenticulostriate arteries or anterior choroidal artery is inadequate.[11] Clarifying relationships between adjacent smaller vessels and lesions is thus difficult using this technique.

Acknowledgments

This work was supported in part by Grants-in-Aid for Advanced Medical Science Research by the Ministry of Education, Culture, Sports, Science, and Technology, Japan (2004–2008).

References

1) Cloft HJ, Joseph GJ, Dion JE: Risk of cerebral angiography in patients with subarachnoid hemorrhage, cerebral aneurysm and arteriovenous malformation: a meta-analysis. *Stroke* 30: 317–320, 1999
2) Heiserman JE, Drayer BP, Keller PJ, Fram EK: Intracranial vascular stenosis and occlusion: evaluation with three-dimensional time-of-flight MR angiography. *Radiology* 185: 667–673, 1992
3) Hochmuth A, Spetzger U, Schumacher M: Comparison of three-dimensional rotational angiography with digital subtraction angiography in the assessment of ruptured cerebral aneurysms. *AJNR Am J Neuroradiol* 23: 1199–1205, 2002
4) Julow J, Major T, Emri M, Valálik I, Sági S, Mangel L, Németh G, Trón L, Várallyay G, Solymosi D, Hável J, Kiss T: The application of image fusion in stereotactic brachytherapy of brain tumours. *Acta Neurochir (Wien)* 142: 1253–1258, 2000
5) Kashimura H, Inoue T, Ogasawara K, Arai H, Otawara Y, Kanbara Y, Ogawa A: Prediction of meningioma consistency using fractional anisotropy value measured by magnetic resonance imaging. *J Neurosurg* 107: 784–787, 2007
6) Sekhar LN, Javed T: Meningiomas with vertebrobasilar artery encasement: review of 17 cases. *Skull Base Surg* 3: 91–106, 1993
7) Shimizu S, Suzuki H, Maki H, Maeda M, Miya F, Benali K, Trousset Y, Taki W: A novel image fusion visualizes the angioarchitecture of the perforating arteries in the brain. *AJNR Am J Neuroradiol* 24: 2011–2014, 2003
8) Stokking R, Zuiderveld KJ, Hulshoff Pol HE, van Rijk PP, Viergever MA: Normal fusion for three-dimensional integrated visualization of SPECT and magnetic resonance brain images. *J Nucl Med* 38: 624–629, 1997
9) Sugahara T, Korogi Y, Nakashima K, Hamatake S, Honda S, Takahashi M: Comparison of 2D and 3D digital subtraction angiography in evaluation of intracranial aneurysms. *AJNR Am J Neuroradiol* 23: 1545–1552, 2002
10) Willinsky RA, Taylor SM, TerBrugge K, Farb RI, Tomlinson G, Montanera W: Neurologic complications of cerebral angiography: prospective analysis of 2899 procedures and review of the literature. *Radiology* 227: 522–528, 2003
11) Wilms G, Bosmans H, Marchal G, Demaerel P, Goffin J, Plets C, Baert AL: Magnetic resonance angiography of supratentorial tumours: comparison with selective digital subtraction angiography. *Neuroradiology* 37: 42–47, 1995
12) Yano S, Kuratsu J; Kumamoto Brain Tumor Research Group: Indications for surgery in patients with asymptomatic meningiomas based on an extensive experience. *J Neurosurg* 105: 538–543, 2006

Address reprint requests to: Hiroshi Kashimura, M.D., Department of Neurosurgery, Iwate Medical University School of Medicine, 19–1 Uchimaru, Morioka, Iwate 020–8505, Japan.
e-mail: hkashi@iwate-med.ac.jp

Commentary

The authors have to be congratulated for having fused the images of MR imaging, with the images of MRA. It is well known that the main problem for the parasagittal meningiomas, and in particular in the parietal region, are the bridging veins and how much they are in conflict with the tumorous lesion. It is, of course, very important also to be aware preoperatively of how the arteries are either incased in the tumor or pushed and stretched away.

This report does represent a very important practical step forward regarding more accurate planning of the surgical procedure in parasagittal meningiomas. In my personal view it is necessary to value the veins equally seriously as the arteries of the region.

Vinko V. DOLENC, M.D.
Department of Neurosurgery
University Medical Center
Ljubljana, Slovenia

The use of various fusion techniques has received considerable attention in the current literature and has started to yield encouraging results in clinical practice. Recent papers have described techniques for fusing 3D DSA images with MR images, PET with CT, PET with MRI and CT with MRI. Fusion techniques provide the information from two different radiological techniques in a single image.

In this paper, the authors describe a novel fusion technique for combining conventional MR imaging and MR angiography to facilitate surgical planning of meningiomas in 10 patients. Two illustrative cases have been discussed. The angiograms are obtained using the 3D TOF technique and fused with SPGR datasets to depict the relationship of the tumor with the intracranial vasculature. The authors have developed volume registration and visualization software to fuse the data on a personal computer.

The major limitation of this technique is inability to resolve smaller vessels and depict their relationship with the tumor. Thus, small vessels like the lenticulostriate vessels and the anterior choroid vessels and their relation to a tumor cannot be depicted. These small vessels can be depicted on a 3D DSA study, which can also be fused with conventional MR images. However, the highlight of this fusion software is that when a vessel is marked as a line on the 3D MR angiogram, it is depicted simultaneously on the axial SPGR image as a red point. This provides a unique anatomical perspective. Furthermore, the software developed by the authors supports images in the DICOM format in which they are acquired, thus limiting post processing times. A significant advantage of this technique is that the fusion imaging can be performed within 15 minutes. These fusion images can facilitate pre-treatment estimation of the functional risks related with vascular injuries by neurosurgical or endovascular treatment of any intracranial lesion.

Thus, fusion of conventional high resolution MR images with 3D MR angiograms described by the authors is an elegant and useful tool for the surgical mapping of the peritumoral angioarchitecture of a meningioma.

Darshana SANGHVI, M.D.
and Atul GOEL, M.D.
Department of Neurosurgery
King Edward VII Memorial Hospital
& Seth G.S. Medical College
Parel, Mumbai, India

In contrast with the less complicated finding of vascular displacement, vascular invasion is one of the most important considerations in the preoperative evaluation to assess the resectability and risk of surgical treatment of complex intracranial tumors, especially meningiomas of the skull base. Kashimura et al. make an important contribution in their documentation that the fusion of magnetic resonance angiography and imaging studies applied preoperatively is of extraordinary value in predicting safe and effective resection of complex meningiomas. The authors report the technique is especially valuable for lesions that involve the proximal branches of the carotid, middle cerebral, and anterior cerebral arteries. At the Mayfield Clinic and the University of Cincinnati Neuroscience Institute, we have corroborated the authors' findings in several critical cases.

John M. TEW, Jr., M.D.
The Neuroscience Institute:
University of Cincinnati College of Medicine
and the Mayfield Clinic
Cincinnati, Ohio, U.S.A.

J Neurosurg 109:811–816, 2008

Transient expansion of vestibular schwannoma following stereotactic radiosurgery

Clinical article

Osamu Nagano, M.D.,[1] Yoshinori Higuchi, M.D., Ph.D.,[1] Toru Serizawa, M.D., Ph.D.,[2] Junichi Ono, M.D., Ph.D.,[3] Shinji Matsuda, M.D.,[4] Iwao Yamakami, M.D., Ph.D.,[1] and Naokatsu Saeki, M.D., Ph.D.[1]

[1]Department of Neurological Surgery, Chiba University Graduate School of Medicine, Chiba; and [2]Gamma Knife House, Departments of [3]Neurosurgery and [4]Neurology, Chiba Cardiovascular Center, Ichihara, Japan

Object. The authors prospectively analyzed volume changes in vestibular schwannomas (VSs) after stereotactic radiosurgery.

Methods. One hundred consecutive patients with unilateral VS treated with Gamma Knife surgery (GKS) at Chiba Cardiovascular Center between 1998 and 2006 were analyzed in this study. For each lesion the Gd-enhanced volume was measured serially every 3 months in the 1st year, then every 6 months thereafter, using volumetric software. The frequency and degree of transient tumor expansion were documented and possible prognostic factors were analyzed. Concurrently, neurological deterioration involving trigeminal, facial, and cochlear nerve functions were also assessed.

Results. The mean observation period was 65 months (range 25–100 months). There were 32 men and 68 women, whose mean age was 59.1 years (range 29–80 years). Tumor volumes at GKS averaged 2.7 cm^3 (range 0.1–13.2 cm^3), and the lesions were irradiated at the mean 52.2% isodose line for the tumor margin (range 50–67%), with a mean dose of 12.2 Gy (range 10.5–13 Gy) at the periphery. The tumor volume was increased by 23% at 3 months and 27% at 6 months. Tumors shrank to their initial size over a mean period of 12 months. The maximum volume increase was < 10% (no significant increase) in 26 patients, 10–30% in 23, 30–50% in 22, 50–100% in 16, and > 100% in 13. The peak tumor expansion averaged 47% (range 0–613%). A high-dose (≥ 3.5 Gy/min) treatment appears to be the greatest risk factor for transient tumor expansion, although the difference did not reach statistical significance. Transient facial palsy and facial dysesthesia correlated strongly with tumor expansion, but only half of the hearing loss was coincident with this phenomenon.

Conclusions. Transient expansion of VSs after GKS was found to be much more frequent than previously reported, strongly suggesting a correlation with deterioration of facial and trigeminal nerve functions.
(DOI: 10.3171/JNS/2008/109/11/0811)

Key Words • **facial nerve function** • **Gamma Knife surgery** • **stereotactic radiosurgery** • **transient tumor expansion** • **trigeminal nerve dysesthesia** • **vestibular schwannoma**

Recently, SRS for small VSs has been established as being efficacious, with high tumor control rates and extremely low incidences of severe complications.[11,18-21,23] However, we occasionally encounter transient cranial neuropathies, such as facial dysesthesia, facial spasm, tinnitus, vertigo, and hearing loss. Typical MR images show initial enlargement with central low intensity within 1 year after treatment, termed "temporary enlargement,"[14] "tumor expansion,"[6,19] or "transient expansion."[4] Thereafter, the tumor volume gradually decreases over a 1-year period. In this study, we prospectively analyzed the frequency and degree of transient expansion, and the relationships between tumor expansion and cranial neuropathies are discussed.

Abbreviations used in this paper: GKS = Gamma Knife surgery; SRS = stereotactic radiosurgery; VS = vestibular schwannoma.

Methods

Patient Population

One hundred consecutive patients with unilateral VS treated with GKS at Chiba Cardiovascular Center between 1998 and 2006 were analyzed in this study. Patient characteristics are shown in Table 1, and radiosurgical parameters in Table 2. There were 32 men and 68 women, with a mean age of 59.1 years (median 59 years, range 29–80 years). Thirty-five patients (35%) had undergone resection.

The SRS was performed using the standard GKS technique.[11,12] The procedure begins with the patient's head being placed in a rigid fixation Leksell G stereotactic frame (Elekta Instruments) after induction of local anesthesia with adequate sedation. Treatment planning was performed using the Leksell Gamma Plan by one

TABLE 1

Characteristics of 100 patients who underwent GKS treatment for VS

Variable	Value
age in yrs	
range	29–80
mean (median)	59.1 (59)
sex (no.)	
male	32
female	68
tumor laterality (no.)	
lt	46
rt	54
no. w/ previous op	35
follow-up period in mos	
range	25–100
mean (median)	65 (66)

neurosurgeon (T.S.) in all cases. For dose planning, we always use contrast-enhanced T1-weighted gradient-echo axial MR sequences (TR 45 msec, TE 3.5 msec, flip angle 30, field of view 260 mm, slice thickness 2 mm, interslice gap 0 mm, and matrix 400 × 382), as well as continuous-interference steady-state sequences and CT scanning. All patients were treated using the Gamma Knife model B (Elekta Instruments). The multiple-isocenter technique was used and the standard prescription dose was 50% 12 Gy in the periphery.

Follow-up neuroimaging included contrast-enhanced T1-weighted gradient-echo MR sequences, the same as those used for dose planning. For each lesion the Gd-enhanced volume was measured serially every 3 months during the 1st year, and 6 months thereafter, using non-invasive volumetric software (GammaPlan or SurgiPlan). The volume measurements were performed by 2 neurosurgeons (T.S. and O.N.). Error was estimated to be < 5%, as verified by phantom studies at another site.[1] We found the margin of error with this method to be ± 5% for lesions in our phantom studies (data not shown). Significant tumor expansion was defined as > 10% enlargement. We defined transient expansion as at least a 10% increase in tumor volume, after SRS, followed by shrinkage. Concurrent neurological deterioration, involving trigeminal, facial, and cochlear nerve functions, was also examined with radiological follow-up by one neurosurgeon (T.S.).

TABLE 2

Radiosurgical parameters in 100 patients with VSs treated with GKS

Variable	Value
tumor vol in cm^3	
range	0.1–13.2
mean (median)	2.7 (2.0)
peripheral dose in Gy	
range	10.5–13.0
mean (median)	12.2 (12.0)
Paddick conformity index	
range	0.43–0.93
mean (median)	0.80 (0.86)
dose rate in Gy/min	
range	1.66–3.67
mean (median)	2.67 (2.73)

Trigeminal neuropathy was defined as any facial dysesthesia within the ipsilateral trigeminal nerve distribution. Facial neuropathy was defined as any deterioration in House–Brackmann facial nerve grade.[7] Acoustic neuropathy was defined as any decline in Gardner–Robertson hearing class[5] for patients with at least Class IV hearing.

The frequency and degree of tumor expansion were documented. The interval between peak expansion and shrinkage to the initial size was analyzed using the Kaplan–Meier method. To analyze prognostic factors, we assessed the following dichotomized variables: age (< 60 vs ≥ 60 years), sex (male vs female), tumor laterality (right vs left), previous surgery (yes vs no), tumor volume (< 2 vs ≥ 2 cm^3), peripheral dose (< 12 vs ≥ 12 Gy), Paddick conformity index[16] (< 0.8 vs ≥ 0.8), and dose rate (< 3.5 vs ≥ 3.5 Gy/min). Factors affecting tumor expansion were evaluated using a logistic regression model. We compared the onsets of these neurological deteriorations between patients with < 30% versus ≥ 30% increment in tumor volume by using the log-rank test. A probability value of < 0.05 was defined as statistically significant.

Results

Radiosurgical Techniques

The tumor volume at GKS averaged 2.7 cm^3 (median 2, range 0.1–13.2 cm^3). The mean peripheral dose was 12.2 Gy (median 12 Gy, range 10.5–13 Gy). The isodose line for the tumor margin varied from 50 to 67% (mean 52.2%, median 50%). Isocenter numbers were 4–42 (mean 16.7, median 17) and the mean Paddick conformity index was 0.80 (range 0.43–0.93).[16] The mean observation period was 65 months (median 66, range 25–100 months).

Maximum tumor expansion rates are shown in Fig. 1. The volume increase was < 10% (no significant increase) in 26 cases, 10–30% in 23, 30–50% in 22, 50–100% in 16, and > 100% in 13. Peak expansion was most frequently observed at 6.4 months after GKS and averaged 47% (range 0–613%) of the initial volume (Fig. 2). Figure 3 demonstrates tumor shrinkage to the initial size. Half the tumors regressed to their initial size within 1 year. Nine percent of tumors were still larger than they had been initially as long as 5 years after treatment. These patients experienced transient expansion, but the tumor remained

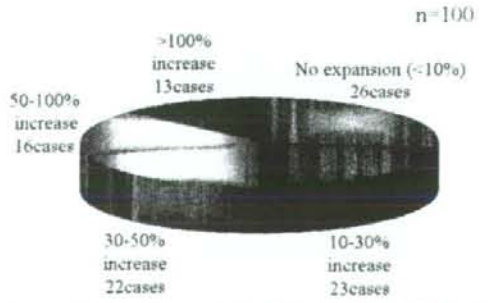

FIG. 1. Pie chart demonstrating the frequency of maximum transient tumor expansion. Volume increases > 100% were seen in 13 patients.

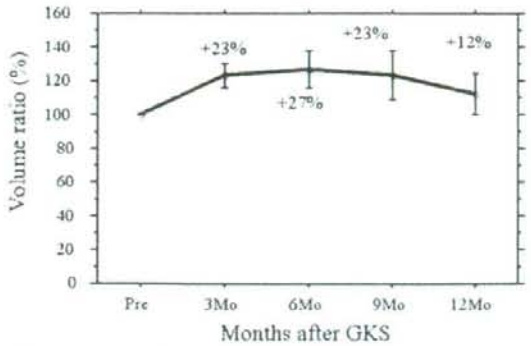

FIG. 2. Graph depicting changes in tumor volume ratios in 100 patients. Tumor volume was increased by 27% at 6 months but had decreased to the initial volume by 18 months postoperatively.

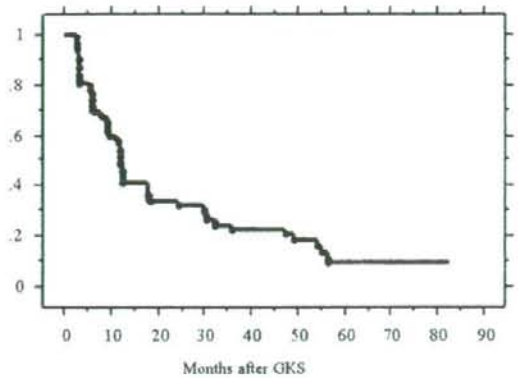

FIG. 3. A Kaplan–Meier curve showing shrinkage to the initial tumor volume in 100 patients. The median survival period was 11.9 months. Nine percent of tumors remained enlarged as long as 5 years after treatment. Values on the y axis denote the tumor shrinkage rate.

larger than the initial volume during follow-up. Tumor volume changes according to age, sex, laterality, previous surgery, tumor volume, peripheral dose, conformity index, and dose rate are presented in Fig. 4. A high dose rate appears to be the greatest risk factor for tumor expansion, but logistic regression did not reveal a statistically significant difference ($p = 0.877$).

There were statistically significant differences in the incidences of trigeminal, facial, and cochlear nerve dysfunctions between patients with tumor expansion < 30% versus ≥ 30% (Fig. 5). Facial dysesthesia was triggered by the tumor attaching to the trigeminal nerve. All MR images of 17 patients with trigeminal neuropathy showed tumor tissue attached to the trigeminal nerve before or after treatment, and in 7 patients this tissue subsequently detached from the trigeminal nerve as the tumor shrank. Improvement of trigeminal neuropathy required a few months after the tumor had been detached from the trigeminal nerve. Twenty patients experienced facial paresis as tumor volume increased. The most common problem of this type was facial spasm (17 patients; 85%). In this study, all patients with facial palsy showed rapid and full recovery to their pre-GKS status, as the tumor shrank. Hearing was preserved in 60% of 28 patients with useful hearing. Half of hearing loss corresponded to tumor expansion, but hearing seldom normalized as the tumor shrank (only 1 patient experienced recovery). The incidence of radiation-induced edema of the cerebellum was 14% in our study. This occurred ~ 6 months after irradiation, corresponding to transient expansion, and decreased as the tumor shrank.

Illustrative Case

This 64-year-old woman had an expanding residual VS after 2 operations. The tumor (3.8 cm^3) was treated with a peripheral dose of 50% 12 Gy (Fig. 6A). The lesion then gradually increased in size (Fig. 6B and C). Nine months after treatment, she experienced facial spasm (House–Brackmann Grade III) and dysesthesia. Admission MR imaging demonstrated that the tumor had doubled in size and showed central low intensity (Fig. 6D). Fifteen months after GKS, expansion was maximal. The tumor was nearly 4 times its original size (Fig. 6E). Thereafter, the tumor shrank to its initial size (Fig. 6F), and continues to shrink (Fig. 6G). The patient recovered from the facial paresis as the tumor regressed over a 2-year period, and facial dysesthesia had nearly disappeared 3 years after GKS.

Discussion

Incidences of transient tumor expansion reportedly range from 17 to 62%.[6,14,20,23,24] In contrast, in this study we found that 74% of patients with VS after GKS show significant transient tumor expansion (≥ 10% increase). This difference is attributable to differing observation periods, measurement methods, and cutoff values. We evaluated tumor volumes using MR imaging every 3 months after GKS with 3D measurements based on GammaPlan or SurgiPlan. In most previous reports, tumor volumes were measured by 2D methods with follow-up imaging at 6 months.[6,14,23] This difference indicates that 2D measurement is not suitable for detecting small changes in volume. For example, a 10% increase in diameter is equivalent to a 33% volume expansion.

We found the incidence of transient expansion, with peak expansion usually being observed at 6–9 months, to represent a volume increase to nearly 50% of the initial volume. Irradiation did induce biological changes in the tumors. We did not clarify the mechanism of transient tumor expansion in this study. Several authors have suggested that increased tumor size after GKS could be caused by radiation-induced tumor necrosis,[20] chronic intratumoral bleeding resulting from delayed radiation injury,[8] and/or a biological response to radiation.[14]

Cranial Nerve Dysfunctions

Recently, there have been several reports on transient expansion after SRS for VS, but little is known about neurological deterioration associated with this phenomenon. In the early 1990s, facial nerve paresis after SRS was

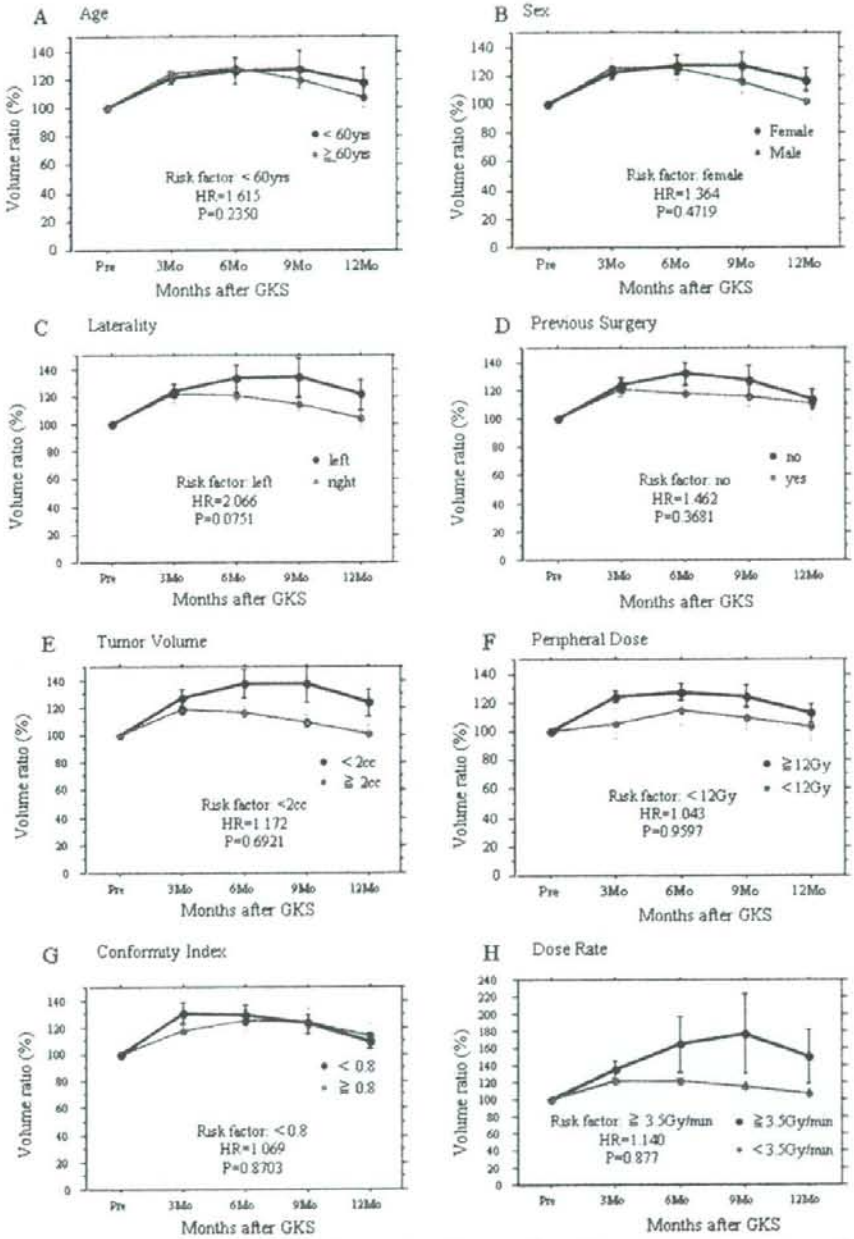

FIG. 4. Graphs showing tumor volume changes according to various factors: age, sex, laterality, previous surgery, tumor volume, peripheral dose, conformity index, and dose rate. A high dose rate seems to be the greatest risk factor for transient expansion. However, logistic regression failed to detect any statistically significant difference. HR = hazard ratio.

considered to result directly from radiation injury, and the treatment dose was thus reduced from 15 Gy to the present 12–13 Gy.[3,17,22] The use of MR imaging for dose planning, combined with CT scanning and improved dose-planning software, has greatly reduced direct radiation injury.[13,15,17] Despite these advances, transient facial spasm does occasionally manifest within 1 year after SRS. In our institute, under close observation, we found that 20% of patients

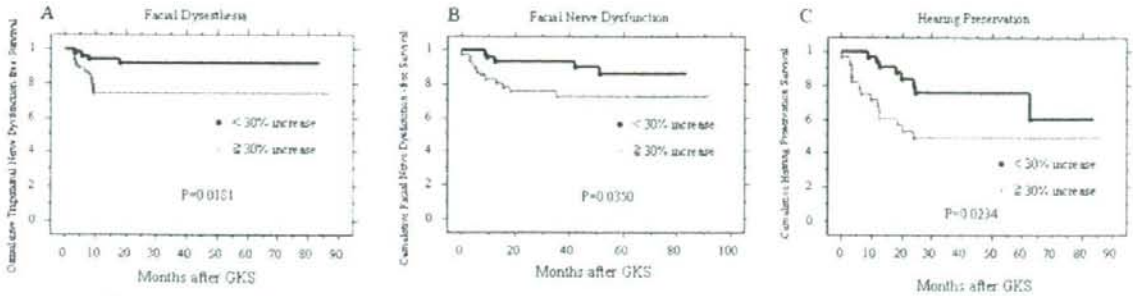

FIG. 5. Kaplan–Meier curves demonstrating the cranial neuropathy-free survival rate based on facial dysesthesia, facial nerve dysfunction, and hearing preservation, comparing patients with a < 30% increase to those with a ≥ 30% increase in tumor volume. The differences are statistically significant.

experienced facial spasm and that it was associated with transient tumor expansion (Fig. 5B). Facial spasm usually started with the lower eyelid, and then extended to the angle of the mouth. This spasm is a temporary phenomenon related to facial paresis, which has been described as facial myokymia.[9,10] The facial spasm disappears as the tumor shrinks.

Trigeminal nerve dysfunction was also strongly related to transient tumor expansion (Fig. 5A). The trigeminal nerve disturbance usually manifested as ipsilateral facial dysesthesia without motor paresis. Patients described the sensation as like anesthesia for a dental procedure or as a pins-and-needles sensation, and typical trigeminal neuralgia was occasionally recognized. This symptom improved as the tumor shrank. However, trigeminal dysesthesia usually improved later than facial paresis, often taking several months or even years to resolve. It is important to inform patients thoroughly about these potential sequelae. Furthermore, we explain to our patients the temporal relationship between transient expansion and these symptoms.

On the other hand, half of hearing loss is attributable to post-GKS deterioration, which is not related to tumor expansion (Fig. 5C). This observation suggests that acoustic nerves may be injured with even lower doses than for the fifth and seventh cranial nerves.[2] However, only 1 of our patients experienced hearing loss after GKS; this patient's hearing normalized as the tumor shrank. To

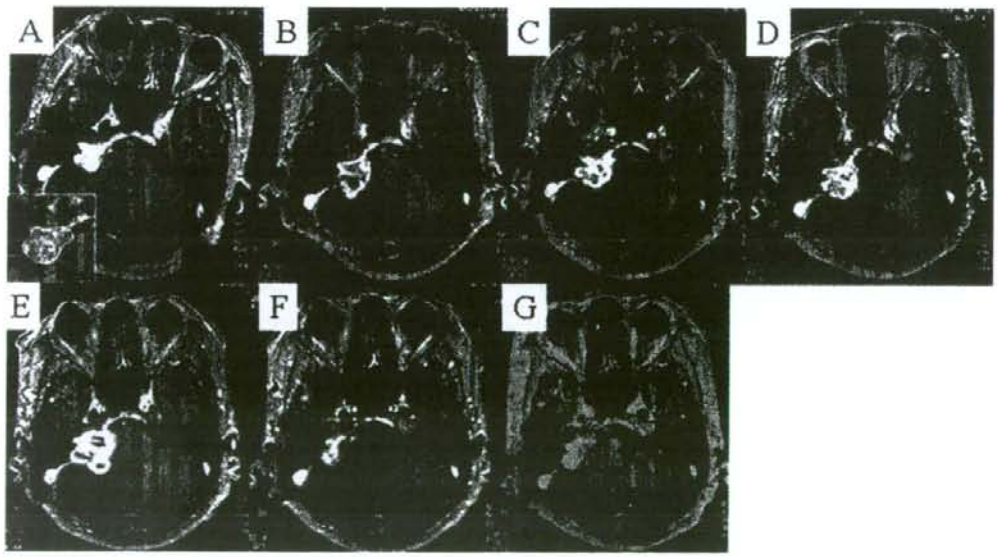

FIG. 6. Serial contrast-enhanced axial T1-weighted MR images obtained in a 64-year-old woman with a right VS who underwent GKS. A: Dose-planning image for a right-sided VS. *Line (inset)* indicates the 50% isodose curve. The initial tumor volume was 3.8 cm^3. B: On an MR image obtained 3 months later, there was an 81% expansion (6.9 cm^3) with central low intensity. C: Image obtained 6 months post-GKS, demonstrating a 97% expansion (7.5 cm^3). D: Image obtained 9 months post-GKS, showing a 105% expansion (7.8 cm^3). E: Image obtained 15 months post-GKS, demonstrating maximum expansion (276%, 14.3 cm^3). F: Image obtained 4 years post-GKS, showing shrinkage to nearly the initial size (3.7 cm^3). G: Image obtained 6 years post-GKS, showing remarkable tumor regression (3.1 cm^3).